Available online at www.sciencedirect.com
SCIENCE DIRECT®
Journal of Power Sources 139 (2005) 21–29
JOURNAL OF POWER SOURCES
www.elsevier.com/locate/jpowsour

A random resistor network analysis on anodic performance enhancement of solid oxide fuel cells by penetrating electrolyte structures

Dong Hyup Jeon, Jin Hyun Nam, Charn-Jung Kim*

School of Mechanical and Aerospace Engineering, Seoul National University, Seoul 151-744, South Korea

Received 16 May 2004; received in revised form 19 June 2004; accepted 13 July 2004
Available online 25 September 2004

Abstract

The anodic performance enhancement of solid oxide fuel cells (SOFCs) by introducing penetrating electrolyte structures was investigated using a random resistor network model considering the transport of electrons and ions, and the electrochemical reaction in composite anodes. The composite anode was modeled as a mixture of ionic and electronic particles, randomly distributed at simple cubic lattice points. The dependence of the anodic polarization resistances on the volume fraction of the electronic phase, the thickness of the anode, and the insertion of various penetrating electrolyte structures were explored to obtain design criteria for best performing composite anodes. The network simulation showed that the penetrating electrolyte structures are advantageous over flat electrolytes by enabling more efficient use of electrochemical reaction sites, and thereby reducing the polarization resistances.

Keywords: Solid oxide fuel cell; Composite anode; Penetrating electrolyte structures; Anodic polarization resistance; Random resistor network model

1. Introduction

SOFC is a high temperature fuel cell that directly converts chemical energy of gaseous fuel and oxidant to electrical energy by electrochemical reaction [1]. A typical SOFC is composed of a composite anode made of nickel (Ni) and yttria-stabilized zirconia (YSZ), and a composite cathode made of lanthanum strontium manganite (LSM) and YSZ, attached to either side of a thin YSZ electrolyte. The performance of SOFC is, therefore, sum of the performance of each component comprising SOFC. The ionic conductivity of YSZ is around 0.1 S cm^{-1} at 1000 °C. The low ionic conductivity of the electrolyte is among main factors that limit the performance of SOFC. With advance in material processing, thinner electrolytes become possible and the problem due to high ohmic loss has been largely overcome. Currently, electrolytes made of YSZ are used for intermediate temperature operation of SOFC at about 800 °C.

While thinner electrolytes generally perform better aside from mechanical problems, that is not true with electrodes. The performances of the anode and the cathode of SOFC are not only governed by the transport of oxygen ions and electrons, but they are also governed by the electrochemical reaction (also by the transport of the gas molecules of fuel and oxidant). The electrochemical reaction is generally accepted to occur at three phase boundaries (TPBs) where all the components required for the electrochemical reaction (oxygen ions, electrons and gas molecules) co-exist by the contact of ionic phase, electronic phase, and gas-diffusing pores. While reducing the thickness of the electrode is favorable for the performance by decreasing the ohmic resistance and by increasing the rate of gaseous diffusion, it also reduces TPBs where the electrochemical reaction occurs, thereby increasing the polarization resistance.

Many studies have been conducted to correlate microstructural parameters and performance of the composite electrodes in order to provide fundamental information for optimization. Using either resistor network models based on regular lattices or random packings [2–4] or continuum

* Corresponding author. Tel.: +82 28801662; fax: +82 28830179.
E-mail address: kimcj@plaza.snu.ac.kr (C.-J. Kim).

0378-7753/$ – see front matter © 2004 Elsevier B.V. All rights reserved.
doi:10.1016/j.jpowsour.2004.07.014

Nomenclature

I_g	current generation (A)
I_{ij}	current flowing from particle i to particle j (A)
I_{tpb}	current generation per TPB (A/# contact)
l	length (μm)
l_p	ion path length or relative distance from the electrolyte (# ionic particle)
n_{tpb}	number of TPBs (# contacts)
R	resistance (Ω)
R_pA	area specific polarization resistance (m Ω cm^2)
R_tA	area specific total resistance (m Ω cm^2)

Greek letters

κ	conductivity (S cm^{-1})
$\sum l_{tpb}$	total TPB length (μm)
$\sum n_{tpb}$	total number of TPBs (# contact)
σ_{ij}	conductance between particle i and particle j (S)
ϕ_{el}	volume fraction of electronic phase
φ	potential (V)

Subscripts

io	ionic phase
el	electronic phase
p	polarization
t	total
tpb	three phase boundary
Ω	ohmic

micro-models based on the statistics of random packings [5–8], criteria for the volume fraction and the size of ionic and electronic particles, and thickness of the composite electrode to obtain optimal performance have been suggested. Recently, an interesting experiment on the cathodic performance enhancement by depositing relatively large YSZ particles onto the surface of the flat electrolyte has been reported by Herbistritt et al. [9]. After a numerical analysis, they proposed that the observed better performance is directly related to the enlargement of the surface area of the electrolyte by the deposited YSZ particles.

By extending the discussion of Herbistritt et al. [9], we proposed penetrating electrolyte structures, the electrolyte structures which are attached to the flat electrolyte and penetrate into the electrode, as an efficient way to enhance the anodic performance. Not to mention the increase in the interfacial area between the electrolyte and the electrode (primary reaction sites) by the penetrating electrolyte structures, they are believed to provide less resistive paths for the transport of oxygen ions towards the interior reaction sites, thereby enhancing the reaction efficiency of TPBs inside the electrode (secondary reaction sites). In this study, a random resistor network model considering the electron conduction in the

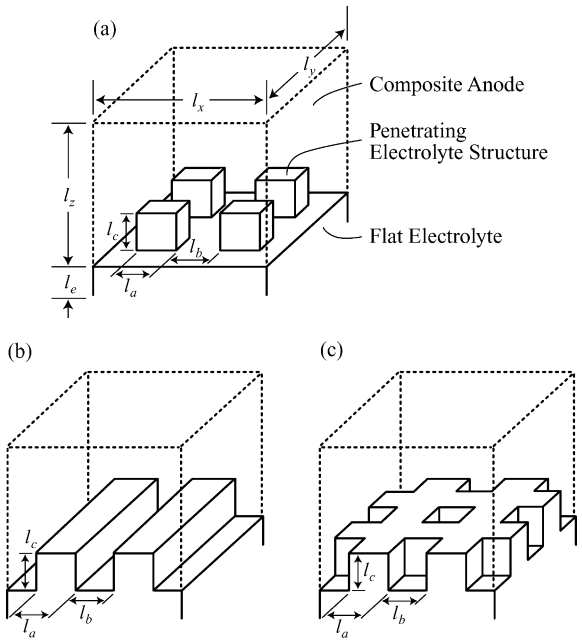

Fig. 1. Three penetrating electrolyte structures proposed in this study. Electrolytes with penetrating block structures (a), rib structures (b), and cross-linked rib structures (c) are shown.

electronic phase, oxygen ion migration in the ionic phase, and the reaction at TPBs formed by the contact of the two phases has been developed to quantitatively assess the anodic performance enhancement by the penetrating electrolyte structures.

2. Random resistor network model

Three penetrating electrolyte structures, proposed in this study, are shown in Fig. 1(a)–(c), where block structures, rib structures and cross-linked rib structures, made of ionic phase, are attached to the surface of the flat electrolytes. Introducing the bulk electrolyte structures that penetrate the composite anode is favorable for the anodic performance by enhancing the oxygen ion transport, thereby facilitating the efficient utilization of TPBs for current generation. The penetrating electrolyte structures are also favorable for the reduction in the concentration polarization by increasing the limiting current density. As the performance enhancement by the proposed penetrating electrolyte structures is purely geometrical, such geometrical modification can be superposed with the invention of new materials to obtain better performance.

From the mechanical point of view, the penetrating electrolyte structures are believed to improve the reliability of SOFC significantly. The penetrating electrolyte structures reduce the volume fraction of electronic phase in the composite electrode, thereby relieving the problem of thermal expansion mismatch between the electrolyte and the electrode. They also facilitate interdigitated close contact at the interface

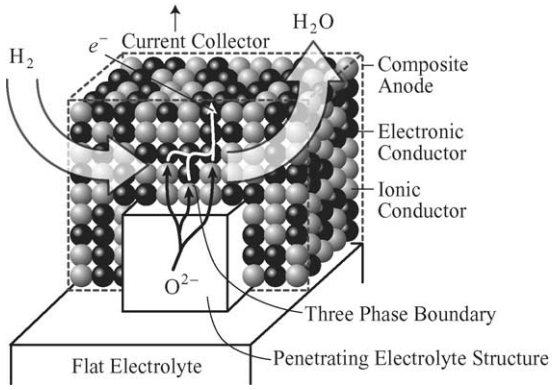

Fig. 2. A random resistor network model for a composite anode. The composite anode is composed of equal-sized ionic and electronic particles, placed on a flat electrolyte with a penetrating electrolyte structure.

between the electrolyte and the electrode, which significantly reduces the possibility of debonding or delamination. The penetrating cross-linked rib structures, especially, can complement small buckling resistances of the electrolytes, making thinner electrolytes possible [10].

The composite anode of SOFC was modeled as a mixture of the ionic particles (white) and electronic particles (black) packed between the electrolyte and the current collector, as shown in Fig. 2. Then, the resistor network was constructed based on the particle network of equal-sized spherical particles, prescribed randomly as either the ionic particle or the electronic particle and placed at the lattice points of a simple cubic lattice. Though the resistor networks based on regular lattices are only approximation of the micro-structures of the real composite anodes, such an approach has been proven to produce reliable prediction when appropriate particle-to-particle resistances are used [2,4].

The electrochemical reaction at the active reaction sites or TPBs requires the oxygen ions migrated from the electrolyte towards TPBs through the network of the ionic particles, and the fuel gas molecules diffused from the channel towards TPBs through pores. Upon completion of the reaction, the resultant electrons are conducted from TPBs towards the current collector through the network of the electronic particles, and the reactant gas molecules are transported back to the channel by diffusion. In order for the above-mentioned processes to happen, the ionic particles and the electronic particles should form continuous networks (percolation) as shown in Fig. 2, assuming the continuous pore network is always available. With negligible diffusion overpotential (concentration loss), the performance of the composite anode solely depends on the transport of ions and electrons, and the electrochemical reaction. In this case, the advantage of the penetrating electrolyte structures in shortening the path for the oxygen ion transport can be easily deduced from Fig. 2.

The governing equations for the conservation of the oxygen ions and electrons are derived from the Kirchhoff's law of current [2]. Current conservations for a particle i connected to a particle j are

$$\sum_{j=\text{ionic}} I^{\text{io}}_{i\to j} = \sum_{j=\text{ionic}} \sigma^{\text{io}}_{ij}(\varphi^{\text{io}}_i - \varphi^{\text{io}}_j) = \sum_{j=\text{electronic}} I^{\text{ct}}_{i\leftarrow j}, \text{ for ionic particle } i \tag{1}$$

$$\sum_{j=\text{electronic}} I^{\text{el}}_{i\to j} = \sum_{j=\text{electronic}} \sigma^{\text{el}}_{ij}(\varphi^{\text{el}}_i - \varphi^{\text{el}}_j) = -\sum_{j=\text{ionic}} I^{\text{ct}}_{i\to j}, \text{ for electronic particle } i \tag{2}$$

where $I_{i\to j}$ is the current flowing from the particle i to the particle j, σ_{ij} is the bond conductance, φ_i and φ_j are the potentials of the particle i and the particle j, respectively, and $I^{\text{ct}}_{i\to j}$ is the charge transfer current due to the electrochemical reaction.

The charge transfer current is a function of the exchange current density, the polarization overpotential, and the reactant and the product concentrations in the anode, as described by Butler-Volmer equation. At low current density, the Butler-Volmer equation can be approximated by a linear charge transfer equation, and the transfer current from the electronic particle i to the ionic particle j is

$$I^{\text{ct}}_{i\to j} = \frac{\eta}{R_{\text{ct}}} = \sigma_{\text{p}}(\varphi^{\text{el}}_i - \varphi^{\text{io}}_j), \tag{3}$$

where R_{ct} is the charge transfer resistance, σ_{p} is the polarization conductance, and η is the polarization overpotential, $\eta = \varphi^{\text{el}} - \varphi^{\text{io}}$.

Combining Eqs. (1)–(3) results in a single form of the current conservation equations, written for a particle i to neighboring particles j as

$$\sum_j I_{i\to j} = \sum_j \sigma_{ij}(\varphi_i - \varphi_j) = 0, \tag{4}$$

where the bond conductance σ_{ij} is defined as $\sigma_{\text{io–io}}$ for the contact of two ionic particles, $\sigma_{\text{el–el}}$ for the contact of two electronic particles, and $\sigma_{\text{io–el}}$ for the contact of an ionic particle and an electronic particle.

The bond conductance is dependent on the geometry of neck formed by the contact of two spherical particles. Based on Sunde [2,3], we assumed that the neck perimeter is equal to the TPB length per contact of dissimilar particles. The bond conductances between the same particles were evaluated using the neck perimeter $l_{\text{io–io}}$ and $l_{\text{el–el}}$, and the ionic conductivity κ_{io} and the electronic conductivity κ_{el}, as

$$\sigma_{\text{io–io}} = \frac{\kappa_{\text{io}} l_{\text{io–io}}}{4}, \quad \sigma_{\text{el–el}} = \frac{\kappa_{\text{el}} l_{\text{el–el}}}{4}. \tag{5}$$

The bond conductance for the contact of dissimilar particles is determined by the sum of ionic, electronic, and polarization

resistances, written as

$$\sigma_{\mathrm{io-el}} = \left(\frac{1}{2\sigma_{\mathrm{io-io}}} + \frac{1}{\sigma_{\mathrm{p}}} + \frac{1}{2\sigma_{\mathrm{el-el}}} \right)^{-1}, \quad (6)$$

where the polarization conductance σ_{p} is defined by the polarization conductivity κ_{p} times TPB length l_{tpb}, as

$$\sigma_{\mathrm{p}} = \kappa_{\mathrm{p}} l_{\mathrm{tpb}}. \quad (7)$$

For the consideration of the penetrating electrolyte structures, the conductance between two cubic electrolyte blocks whose length is same as the diameter of the spherical particle d_{s} is necessary. That is

$$\sigma^{B}_{\mathrm{io-io}} = \kappa_{\mathrm{io}} d_{\mathrm{s}}. \quad (8)$$

3. Calculation

Geometrical and electrochemical parameters used for the random resistor network simulations are summarized in Table 1. The electrochemical parameters were from Sunde [2,3] as they were proven to produce results consistent with published experimental observations. For example, the ionic conductivity of YSZ and the electronic conductivity of Ni are standard electrical conductivities measured at the temperature of 1000 °C (0.1 S cm^{-1} for YSZ and 2×10^4 S cm^{-1} for Ni). Only the composite anode composed of equal-sized ionic and electronic particles was considered due to the limitation of the regular lattice. However, such calculation based on the regular lattice is believed to be useful for detecting important features of the transport and reaction in random particle systems.

The numerical simulations were conducted by solving the current conservation equation of Eq. (4) for each percolated ionic and electronic particles. The linearity of the resistor network system enables the arbitrary choice of the potentials as boundary conditions, the potentials at the top φ_{top} and at the bottom boundaries φ_{bot}. By prescribing the potential difference of unity between the top and the bottom boundaries ($\varphi_{\mathrm{top}} - \varphi_{\mathrm{bot}} = 1$), the distribution of the potential in the composite anode was determined. For the solution of the system of governing equations, the method of successive substitution was used with Gauss–Seidel iterative solver. The convergence of the potential was judged by the divergence of the current for all percolated particles i to be smaller than a predetermined value as

$$\sum_j I_{i \to j} = \sum_j \sigma_{ij}(\varphi_i - \varphi_j) < \varepsilon, \quad (9)$$

where the convergence criterion ε was 10^{-14} A.

Once the potential distribution was obtained, the currents flowing through the top and the bottom boundaries were calculated by adding currents through all particles adjacent to the boundaries. The total current flowing through the composite anode I_{t} was determined by averaging the currents calculated at the top and the bottom boundaries. The total electrical resistance R_{t} was estimated as

$$R_{\mathrm{t}} + R_{\mathrm{e}} = \frac{\varphi_{\mathrm{top}} - \varphi_{\mathrm{bot}}}{I_{\mathrm{t}}} = \frac{1}{I_{\mathrm{t}}}, \quad (10)$$

where R_{e} is an electrical resistance of an electrolyte layer which was included to reduce the effect of an equi-potential condition at the bottom boundary. In the simulation, the thickness of the electrolyte layer was fixed to 20 μm ($l_{\mathrm{e}} = 20$ μm), and R_{e} was calculated by

$$R_{\mathrm{e}} = \frac{l_{\mathrm{e}}}{\kappa_{\mathrm{io}} A} = \frac{l_{\mathrm{e}}}{\kappa_{\mathrm{io}} l_x l_y}. \quad (11)$$

Sunde [2,3] has proposed a way to single out the polarization resistance R_{p} from the total resistance R_{t}. By setting the polarization conductivity to be infinite ($\kappa_{\mathrm{p}} = \infty$), the ohmic resistance R_Ω was evaluated at the first hand. Then, the polarization resistance R_{p} was determined from $R_{\mathrm{p}} = R_{\mathrm{t}} - R_\Omega$, where R_{t} was the total resistance obtained from simulations with an appropriate polarization conductivity κ_{p}. However, it is rather insignificant to distinguish the polarization resistance from the total resistance once percolation in the electronic particles is achieved. When the volume fraction of electronic phase in the electrode is sufficiently large ($\phi_{\mathrm{el}} > 0.3$), the ohmic resistance R_Ω becomes small compared with the total resistance.

Table 1
Geometric and electrochemical parameters for random resistor network simulation

Parameter	Value	Description
d_{s}	2 μm	Diameter of spherical particle
l_x, l_y	40 μm	Length of electrode in x- and y-direction
l_z	50 μm	Thickness of electrode
l_{e}	20 μm	Thickness of electrolyte layer
l_{a}, l_{b}	20 μm	Lengths for definition of penetrating electrolyte structures in x- and y-direction
l_{c}	20 μm	Height of penetrating electrolyte structures
l_{tpb}	3 μm	TPB length per contact, $l_{\mathrm{tpb}} = 3 \times (0.5 d_{\mathrm{s}})$
$l_{\mathrm{io-io}}$, $l_{\mathrm{el-el}}$	3 μm	Neck perimeter between ions and electrons
κ_{el}	2×10^4 S cm^{-1}	Conductivity of electronic phase (Ni)
κ_{io}	0.1 S cm^{-1}	Conductivity of ionic phase (YSZ)
κ_{p}	10^{-4} S cm^{-1}	Polarization conductivity with respect to TPB length
ϕ_{el}	0–1	Volume fraction of electronic phase

4. Results and discussions

4.1. Performance enhancement by penetrating electrolyte structures

Fig. 3 shows the calculated area specific resistances $R_{\mathrm{p}}A$ of the composite anodes, with and without the penetrating electrolyte structures, as functions of the volume fraction of electronic phase ϕ_{el}. The results presented as symbols in Fig. 3 are averages of 10 results for each simulated ϕ_{el} with different random seed numbers. The area specific polarization

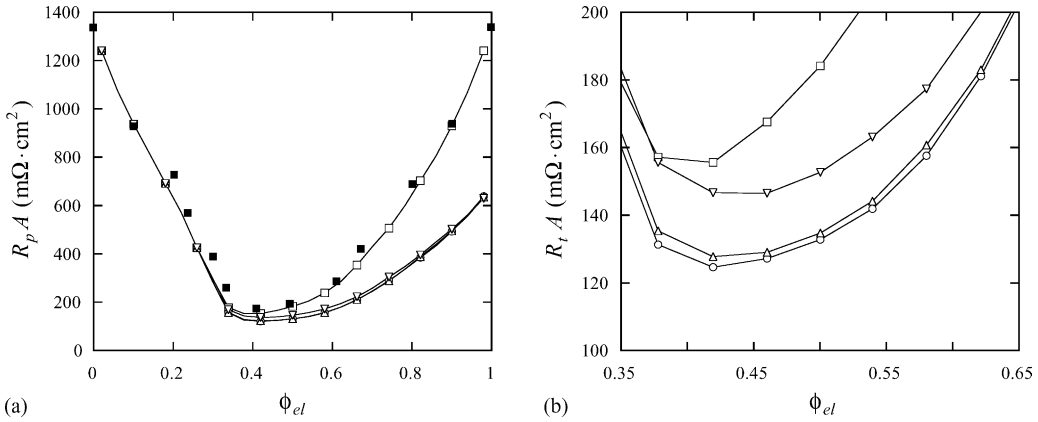

Fig. 3. Area specific polarization resistances R_pA (a) and total resistances R_tA (b), with respect to the volume fraction of electronic phase ϕ_{el}. Symbols with solid lines represent the flat electrolyte (□), and the electrolytes with penetrating block structures (◯), rib structures (△), and cross-linked rib structures (▽). The result for the flat electrolyte by Sunde [2] is also plotted for comparison by a symbol (■) with no line.

resistance R_pA without the penetrating electrolyte structures, shown in Fig. 3(a), is in good agreement with the result by Sunde [2], where small discrepancy can be partially attributed to the dispersion of data in Monte-Carlo simulation. In addition, the present calculations excluded the particles that do not belong to the percolated clusters, and this approach is different from that of Sunde [2,3].

All polarization resistances, shown in Fig. 3(a), exhibit similar trends with respect to ϕ_{el}. Starting from high value, each polarization resistance reaches its minimum at $0.4 < \phi_{el} < 0.5$, and then increases again. Such behaviors are closely related to the total number of TPBs $\sum n_{tpb}$ shown in Fig. 4(a). As polarization conductance κ_p is relatively small compared with the electronic and the ionic conductivities, the overall anodic performance is governed most by total TPB length $\sum l_{tpb}$ ($=\sum n_{tpb} \times l_{tpb}$). Therefore, minimum resistance or maximum performance is generally observed at $\phi_{el} \approx 0.5$ where $\sum l_{tpb}$ becomes largest. Slight discrepancy between ϕ_{el} for minimum resistance and that for maximum $\sum l_{tpb}$ is due to large difference in conductivities of the ionic and electronic phases.

Fig. 3(a) shows that the penetrating electrolyte structures reduce the polarization resistance and thus enhance the anodic performance, especially when ϕ_{el} is large. As noted by Herbistritt et al. [9], one reason for the performance enhancement is related to the surface enlargement by the penetrating electrolyte structures. All three penetrating electrolyte structures, shown in Fig. 1(a)–(c), were found to double the surface area of the electrolyte when their dimensions were set according to Table 1. In case $\phi_{el} > 0.7$, the ionic phase cannot achieve a global percolation and TPBs are spatially restricted in the vicinity of the electrolyte surface. That results in $\sum n_{tpb}$ directly proportional to the surface area of the electrolyte, as shown in Fig. 4(a). As ϕ_{el} approaches 1, three polarization resistance curves with the penetrating electrolyte structures fall into one line, about half of that with the flat electrolyte (without the penetrating electrolyte structures).

The area specific total resistances R_tA are shown in Fig. 3(b) for $0.35 < \phi_{el} < 0.65$, where percolation of both ionic and electronic phases is ensured. Minimum R_tA is observed at $0.4 < \phi_{el} < 0.45$ and the reduction is estimated as much as 20% in case the penetrating block structures are

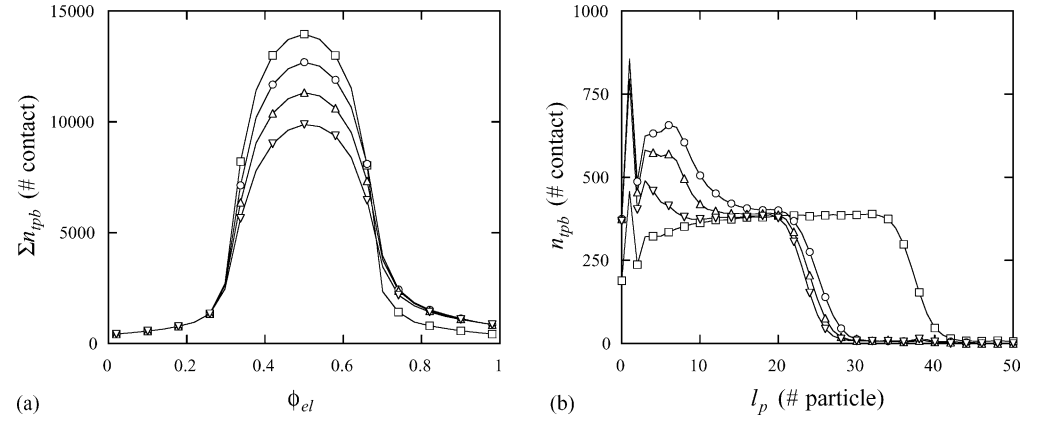

Fig. 4. Total number of TPBs $\sum n_{tpb}$ with respect to the volume fraction of electronic phase ϕ_{el} (a), and the spatial distribution of TPBs n_{tpb} for $\phi_{el} = 0.5$ with respect to the ion path length l_p (b). Symbols represent the flat electrolyte (□), and the electrolytes with penetrating block structures (◯), rib structures (△), and cross-linked rib structures (▽).

considered. Though the surface enlargements by the three penetrating electrolyte structures are same, the sacrifice of the total TPB length $\sum l_{tpb}$ due to the addition of bulk ionic phase is different, which causes difference in the anodic performance enhancement.

For a closer inspection of the performance enhancement by the penetrating electrolyte structures, the spatial distribution of TPBs n_{tpb} as a function of the relative distance from the electrolyte was investigated. For this purpose, each percolated ionic particle was labeled by an ion path length l_p which was defined as the minimum number of ionic particles for ions to travel through to reach the bulk electrolyte phase, counting itself as 1. Then, the number of TPBs was added for the ionic particles with the same l_p, to obtain the distribution of TPBs $n_{tpb}(l_p)$. The TPBs formed by direct contacts of the percolated electronic particles onto the surface of the electrolyte were assigned to $n_{tpb}(0)$.

Fig. 4(b) suggests that the penetrating electrolyte structures change the spatial distribution of TPBs, i.e., the shape of $n_{tpb}(l_p)$; they increase TPBs that have shorter ion path lengths at the sacrifice of TPBs that have longer ion path lengths. The change of the spatial distribution of TPBs is another reason for the performance enhancement by the penetrating electrolyte structures. The three penetrating electrolyte structures result in different degrees of change; largest for the penetrating block structures, and smallest for the penetrating cross-linked rib structures. Therefore the total area specific resistances with the penetrating block structures are smallest as shown in Fig. 3(b).

The current generation with respect to the ion path length $I_g(l_p)$ is shown in Fig. 5(a). It is observed that about 75% of the total current is produced by TPBs whose ion path lengths are less than 10 particles ($l_p \leq 10$) in case of the flat electrolyte. When the penetrating electrolyte structures are introduced, the percentage goes up to 85%. By dividing the current generation by the number of TPBs as $I_g(l_p)/n_{tpb}(l_p) \equiv I_{tpb}(l_p)$, the current generation efficiency of TPBs as a function of the ion path length is investigated. As shown in Fig. 5(b), the current generation efficiency $I_{tpb}(l_p)$ is an exponentially decaying function that decreases about 50% at every increase of the ion path length by 5 particle unit. That is to say, TPBs at the electrolyte surface produce about four times more current than TPBs of the ion path length of 10 particle unit ($I_{tpb}(0) \approx 4I_{tpb}(10)$). As TPBs that have shortest ion path length are most effective, rather small difference in performance enhancement by three penetrating electrolyte structures, shown in Fig. 3(b), can be explained.

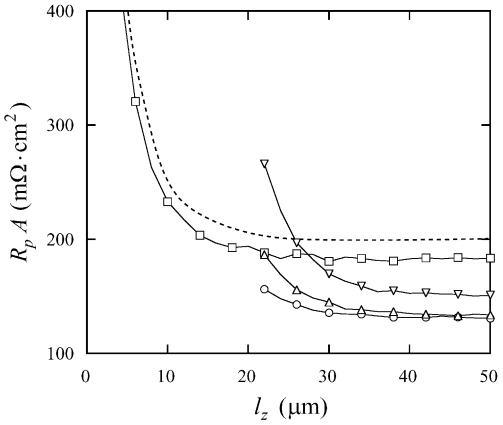

Fig. 6. Area specific polarization resistances R_pA with respect to the electrode thickness l_z for ϕ_{el} = 0.5. Symbols represent the flat electrolyte (□), and the electrolytes with penetrating block structures (◯), rib structures (△), and cross-linked rib structures (▽).

Variation of the area specific polarization resistance R_pA according to the thickness of the composite electrode l_z at ϕ_{el} = 0.5 is shown in Fig. 6. The calculated polarization resistance for the flat electrolyte shows a good agreement with the theoretical prediction by Kenjo et al [11], which is expressed as

$$R_p = \frac{\varphi_0}{I_0} = \sqrt{\rho k}\coth\sqrt{\frac{\rho}{kl}}, \tag{12}$$

where φ_0 and I_0 are the potential difference and the current, ρ is the resistivity of the electrolyte, and l is the electrode thickness. In Fig. 6, all polarization resistances initially decrease

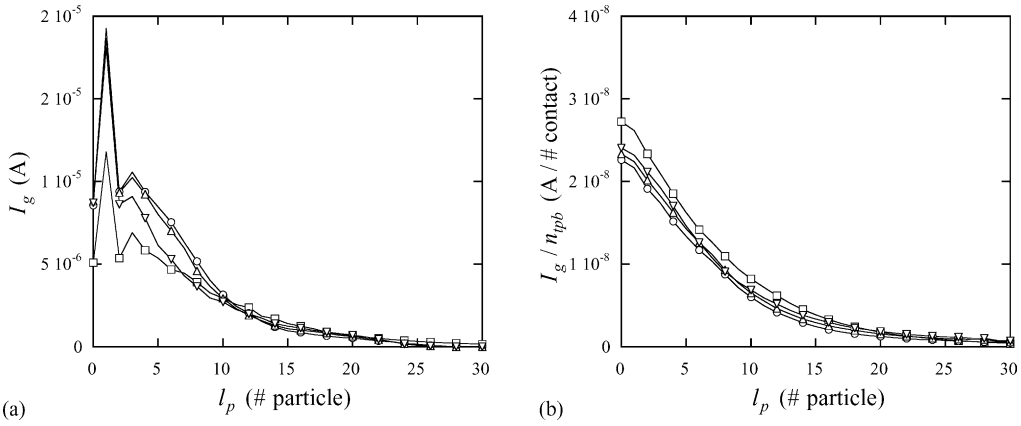

Fig. 5. Distribution of current generation I_g (a) and the current generation per TPB I_g/n_{tpb} (b), for ϕ_{el} = 0.5 with respect to the ion path length l_p. Symbols represent the flat electrolyte (□), and the electrolytes with penetrating block structures (◯), rib structures (△), and cross-linked rib structures (▽).

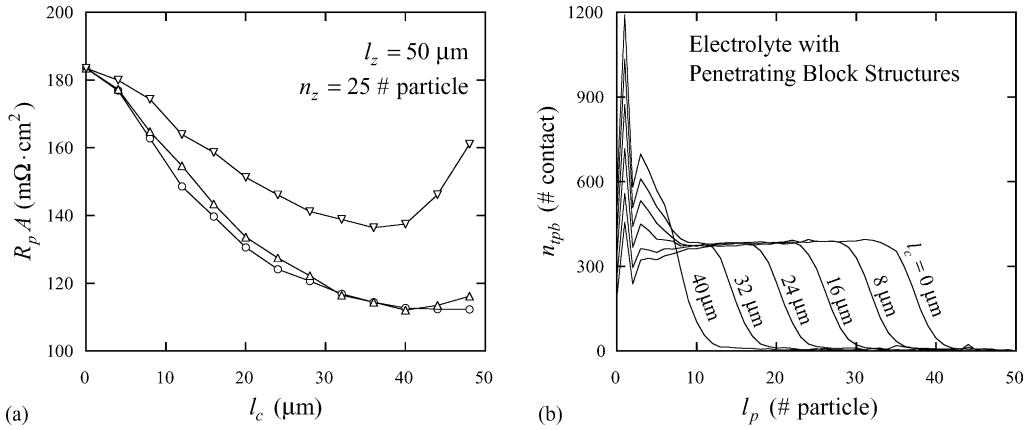

Fig. 7. Area specific polarization resistances R_pA (a) and change of the spatial distribution of TPBs (b), with respect to the heights of the penetrating electrolyte structures l_c, for ϕ_{el} = 0.5 and l_z = 50 μm. Symbols represent the electrolytes with penetrating block structures (◯), rib structures (△), and cross-linked rib structures (▽).

with the increase of the anode thickness and then remain rather constant. When the thickness of the composite anode is small, TPBs in the anode are limited in number; this results in large polarization loss and resistance. However, once sufficient number of TPBs is ensured, an additional increase of the anode thickness does not reduce the polarization resistance. For the flat electrolyte, TPBs in the anode become sufficient for the electrochemical reaction when the anode thickness l_z is larger than 20 μm. In Fig. 5(a), the current produced by TPBs that have less than 20 particle unit ($l_p \leq 20$) amounts more than 90% of total current.

4.2. Optimum design of penetrating electrolyte structures

As a first step for the optimization of the penetrating electrolyte structures, the behaviors of the area specific polarization resistances R_pA of the composite anode with varying height l_c are shown in Fig. 7(a). The anodic polarization resistance with the penetrating rib structures reaches minimum at $l_c \approx 40$ μm while that with the penetrating block structures remains constant for $l_c > 40$ μm. The polarization resistance with the penetrating cross-linked rib structures shows a distinctive minimum at $l_c \approx 35$ μm.

The distributions of TPBs with respect to the ion path length l_p are shown in Fig. 7(b), for different heights l_c of the penetrating block structures. Increasing the height of the penetrating block structures continuously increases TPBs whose ion path length is smaller than 10 particle unit while decreasing TPBs that have the longest ion path length. Since TPBs with smaller ion path length are more efficient in electrochemical reaction and current generation, the anodic performance increases with the increase of the height of the penetrating block structures. The spatial distribution of TPBs shows that the ion path lengths of all TPBs are within 20 particle unit for the block height of 32 μm, and within 10 particle unit for the block height of 40 μm. Then, further increase of the height of the penetrating block structures cannot improve

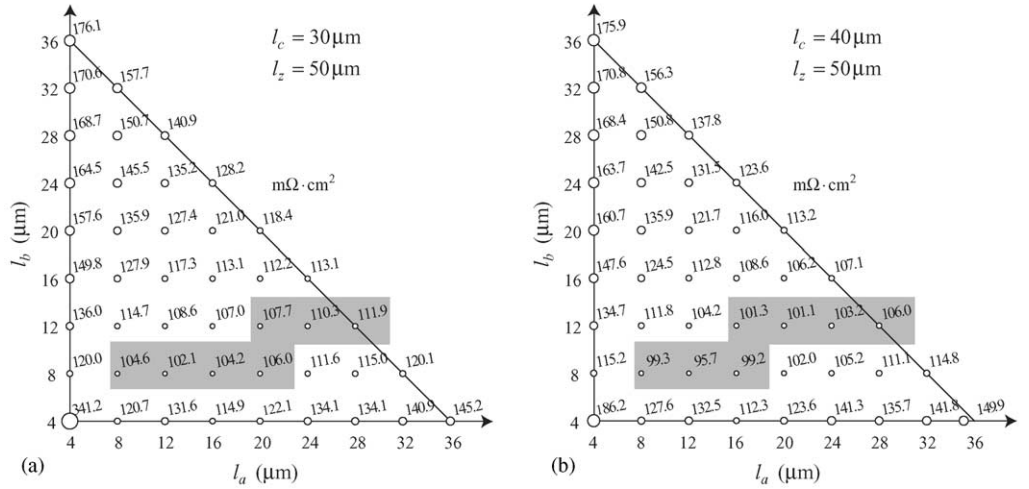

Fig. 8. Area specific polarization resistance R_pA of the composite anode with penetrating block structures for ϕ_{el} = 0.5. The heights of the penetrating block structures l_c are 30 μm (a) and 40 μm (b), and the thickness of composite anode l_z is 50 μm.

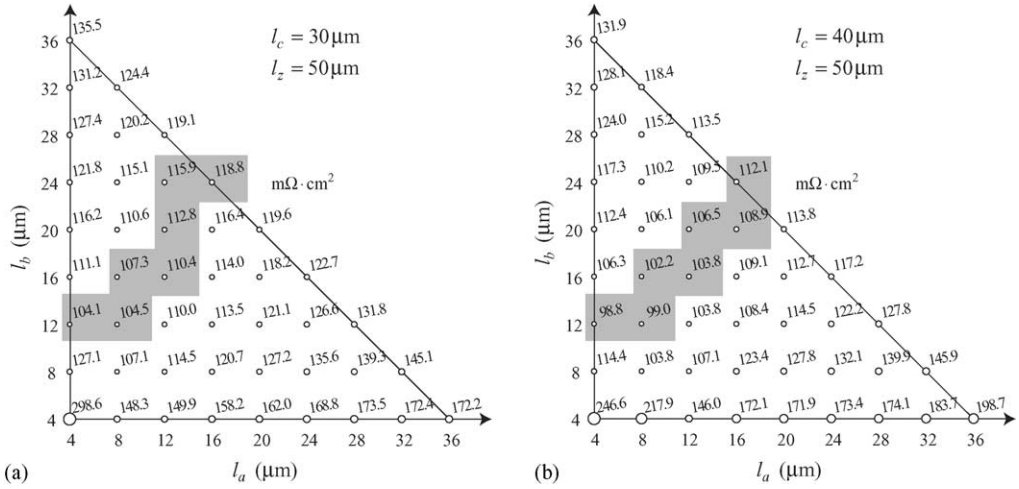

Fig. 9. Area specific polarization resistance R_pA of the composite anode with penetrating rib structures for $\phi_{el} = 0.5$. The heights of the penetrating rib structures l_c are 30 μm (a) and 40 μm (b), and the thickness of composite anode l_z is 50 μm.

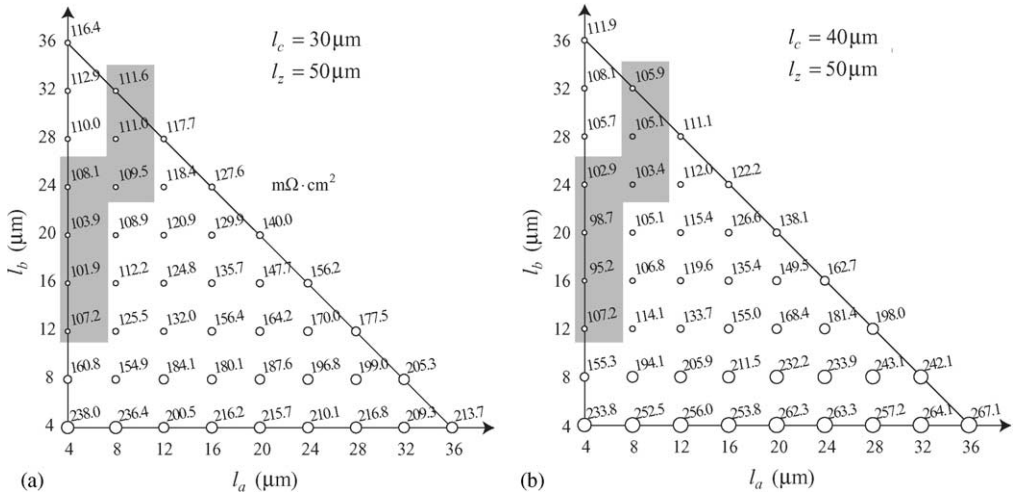

Fig. 10. Area specific polarization resistance R_pA of the composite anode with penetrating cross-linked rib structures for $\phi_{el} = 0.5$. The heights of the penetrating cross-linked rib structures l_c are 30 μm (a) and 40 μm (b), and the thickness of composite anode l_z is 50 μm.

the anodic performance and may deteriorate the performance on the contrary.

From Fig. 7, the criterion for the height of penetrating electrolyte structures (for 50 μm thick composite anode) is identified and the heights of 30 and 40 μm are chosen for further optimization. The polarization resistances obtained by varying the planar dimensions of the penetrating electrolyte structures, l_c and l_b, are shown in Figs. 8–10. It is found that about 40–45% reduction in the anodic polarization resistance can be achieved by the optimization of the planar dimensions and the difference in the minimum resistances with three penetrating electrolyte structures is rather small; 99 m Ω cm^2 for the penetrating block and rib structures, and 95 m Ω cm^2 for the penetrating cross-linked rib structures, compared with 184 m Ω cm^2 for the flat electrolyte. The minimum polarization resistances are also rather insensitive to the height of the penetrating electrolyte structures, resulting only about 5% difference for the height of 30 and 40 μm. The optimum anodic performance with the penetrating block structures is achieved when $l_a > l_b$, while that with the penetrating cross-linked rib structures is achieved when $l_a < l_b$. The penetrating rib structures are found to perform best when $l_a \approx l_b$. When the ratio l_b/l_a is equal, the penetrating electrolyte structures with smaller $l_a + l_b$ perform better, for the surface enlargement is larger.

5. Conclusions

Attachment of the penetrating electrolyte structures to the conventional flat electrolytes of SOFCs was proposed, and the reduction in the anodic polarization resistances was quantitatively assessed using a random resistor network model. The predicted dependency of the anodic performance on microstructural parameters is consistent with the results in the literature, showing that the anodic performance is mainly

governed by the reaction efficiency and the total TPB length of the composite anode. The best anodic performances were obtained when the volume fraction of electronic phase is between 0.4 and 0.5, and when the thickness of the anode is sufficiently large.

The simulation results demonstrated that the penetrating electrolyte structures could reduce the anodic polarization resistance considerably. From the investigation on the distribution of TPBs, the shift in the spatial distribution due to the penetrating electrolyte structures is identified as the main mechanism for the anodic performance enhancement. While total TPB length is reduced by the introduction of the penetrating electrolyte structures, TPBs that are close to the electrolyte surface are increased at the sacrifice of TPBs that are farthest from the electrolyte surface. As the current generation efficiency of TPBs is found to be the exponentially decreasing function of the distance from the electrolyte surface, such change in the spatial distribution of TPBs is favorable for the anodic performance.

A parametric study was conducted to derive design criteria for the dimensions of the penetrating electrolyte structures to obtain optimal anodic performance. Larger height of the penetrating electrolyte structures is favorable for the anodic performance by facilitating easy penetration of oxygen ions into the composite anode as well as by increasing the surface area of the electrolyte more. Optimal heights of the penetrating electrolyte structures are estimated to be between 60 and 80% of the thickness of the composite anode. As to the optimal ranges for the planar dimensions, minimum polarization resistances are achieved, when $l_a > l_b$ for the penetrating block structures, when $l_a < l_b$ for the penetrating cross-linked rib structures, and when $l_a \approx l_b$ for the penetrating rib structures.

References

[1] N.Q. Minh, J. Am. Ceram. Soc. 76 (1993) 563.
[2] S. Sunde, J. Electrochem. Soc. 142 (1995) L50.
[3] S. Sunde, J. Electrochem. Soc. 143 (1996) 1930.
[4] J. Abel, A.A. Kornyshev, W. Lehnert, J. Electrochem. Soc. 144 (1997) 4253.
[5] P. Costamagna, P. Costa, V. Antonucci, Electrochim. Acta 43 (1998) 375.
[6] P. Costamagna, M. Panizza, G. Cerisola, A. Barbucci, Electrochim. Acta 47 (2002) 1079.
[7] S.H. Chan, Z.T. Xia, J. Electrochem. Soc. 148 (2001) A388.
[8] X.J. Chen, S.H. Chan, K.A. Khor, Electrochim. Acta 49 (2004) 1851.
[9] D. Herbistritt, A. Weber, E. Ivers-Tiffee, J. Eur. Ceram. Soc. 21 (2001) 1813.
[10] V.T. Srikar, K.T. Turner, T.Y. Andrew Ie, S.M. Spearing, J. Power Sources 125 (2004) 62.
[11] T. Kenjo, S. Osawa, K. Fujikawa, J. Electrochem. Soc. 138 (1991) 349.